Isolation of Hole Versus Electron Current at p-Si/TiO_2 Selective Contact Using a Heterojunction Bipolar Transistor Structure

Janam Jhaveri, *Student Member, IEEE*, Alexander H. Berg, *Student Member, IEEE*, and James C. Sturm, *Fellow, IEEE*

***Abstract*—Carrier-selective contacts provide an exciting avenue for developing high-efficiency, low-cost silicon photovoltaics (PV). However, evaluating and understanding the different current mechanisms across a carrier-selective contact is difficult as the current measured represents the sum of both electron and hole current components. In this paper, we develop a heterojunction bipolar transistor (HBT) structure with the electron-selective p-type Si/titanium dioxide(TiO_2)/Al contact as the base–emitter junction, which enables one to separately measure the electron and hole currents across the selective contact. An HBT with a current gain as large as ∼220 is achieved. The method is then used to evaluate the current mechanisms across a p-Si/TiO_2/Al heterojunction PV cell, where the TiO_2/p-Si replaces the n^+-p junction. We determine that there is an optimal TiO_2 thickness of 4.1 nm for CVD-deposited TiO_2; and at the optimal thickness, the hole current is 8% of the total current, thus demonstrating that TiO_2/Si is indeed a hole-blocking electron-selective contact. The hole current ratio is corroborated with reverse-recovery experiments, confirming the validity of the HBT method.**

***Index Terms*—Heterojunction, heterojunction bipolar transistor (HBT), photovoltaics, selective contact, silicon, titanium dioxide.**

I. Introduction

HETEROJUNCTION carrier-selective contacts, utilized to replace either p-n or n-n^+ junctions, are of high interest for silicon photovoltaics [1]. Recently, materials such as amorphous silicon [2], [3], poly(3,4-ethylenedioxythiophene):polystyrenesulfonate [4], titanium oxide (TiO_2) [5]–[8], nickel oxide [9], and molybdenum oxide [10] have been investigated for selective contact purposes on silicon. Carrier-selective contacts work by blocking one type of carrier in one direction while allowing the other carrier to pass through (thus selecting one carrier). As such, quantifying the electron and hole current components separately across a terminal could be important to optimize selective contacts. Yet understanding the fundamental performance of such contacts in photovoltaic devices is difficult, because the device current at either contact represents the sum of the electron and hole current at that contact. Thus, determining which current component is dominant, and how small the smaller current is, is not feasible.

In this paper, we introduce a general method using the selective contact in a heterojunction bipolar transistor (HBT) structure, which allows the independent and direct measurement of the electron and hole current components at the selective contact. This paper focuses on the p-type crystalline Si/ TiO_2 contact, but the method is general. We show that in an Al/TiO_2/p-type Si single junction cell with an optimal TiO_2 thickness of 4.1 nm, the hole current is 8% of the total current.

This paper is an extended manuscript based on [11]. New work here includes improved HBT performance as shown by a higher current gain, the ability to isolate one current component as low as 8% of the total current, extraction of an optimal thickness of TiO_2 for selective contact performance, and correlation between HBT and photovoltaic results.

II. Current Processes at p-Si/TiO_2 Heterojunctions

Because of its large band offset compared with silicon (∼2 eV), one can consider using the p-Si/TiO_2 heterojunction as an electron- selective contact on p-Si to replace an n-p junction [5]. This would allow Si-based solar cell fabrication using a low-temperature (∼100 °C) CVD step to replace the high-temperature phosphorus diffusion process. The high offset should ideally block all hole current from the Si toward the cathode in forward bias, enabling the ideal electron injection current (process 1 in Fig. 1) to dominate the current across the junction. However, second-order effects such as recombination at TiO_2/Si interface states (process 2 in Fig. 1) and tunneling either through the TiO_2 or to TiO_2 defect states (processes 3 in Fig. 1) would lead to hole current and could negate the blocking effects of the valence band barrier.

Fig. 2 shows the dark J–V curve of an Al/TiO_2/p-Si diode on a high-lifetime floatzone (FZ) substrate. The TiO_2 is deposited using a low-temperature chemical vapor deposition method (maximum substrate temperature of 100 °C) using titanium tert-butoxide as the precursor [12]. In addition, shown is the ideal

Manuscript received October 11, 2017; revised December 17, 2017 and February 8, 2018; accepted March 16, 2018. Date of current version April 19, 2018. This work was supported by the National Science Foundation under MRSEC Grant DMR-1420541. *(Corresponding author: Janam Jhaveri.)*

The authors are with the Department of Electrical Engineering and Princeton Institute for the Science and Technology of Materials, Princeton University, Princeton, NJ 08544 USA (e-mail: jjhaveri@princeton.edu; ahberg@princeton.edu; sturm@princeton.edu).

Digital Object Identifier 10.1109/JPHOTOV.2018.2819667

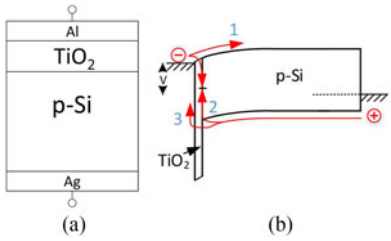

Fig. 1. (a) Device structure and (b) fundamental dark current mechanisms under forward bias (V), with arrows indicating directions of electron and hole flow at a p-Si/TiO_2/Al selective contact [8]. Process 1 is the ideal electron injection current, process 2 is recombination at the Si/TiO_2 interface, and process 3 is hole current through the TiO_2 through either tunneling or defect states.

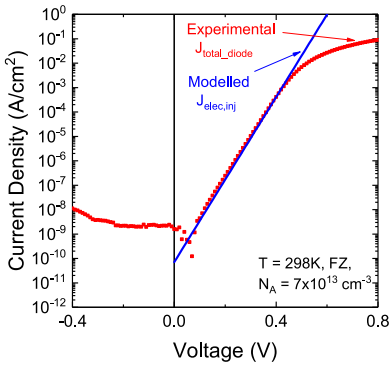

Fig. 2. Measured J–V characteristics of FZ p-Si/TiO2/Si (red) and modeled ideal J–V characteristics for injected electron current (blue). TiO_2 thickness is 4 nm. Positive voltage is on the substrate back contact.

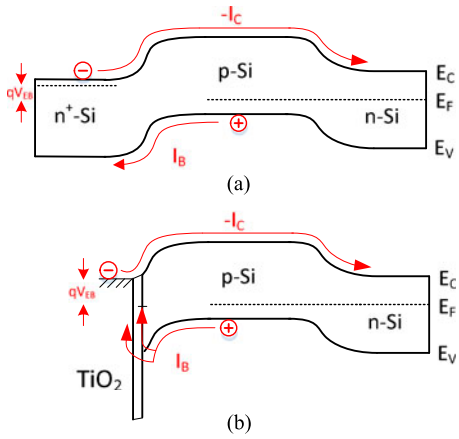

Fig. 3. (a) n-p-n BJT band diagram and current processes and (b) TiO_2/p-n HBT band diagram and current processes.

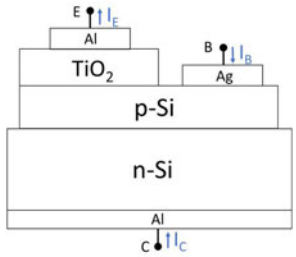

Fig. 4. Cross section of HBT device with n-type Si substrate, p-type Si base, and Al/TiO_2 electron-selective contact to the base as the minority carrier emitter.

injected electron current of electrons ($J_{\text{elec,inj}}$), calculated from

$$J_{\text{elec,inj}} = \frac{qn_i^2 D_n}{N_A W}\left(e^{\frac{qV}{kT}} - 1\right) = J_{0,e} * \left(e^{\frac{qV}{kT}} - 1\right) \qquad (1)$$

where n_i is the intrinsic carrier density, D_n is the diffusion coefficient for electrons in p-Si, N_A is the doping of the p-Si substrate, V is the applied voltage across the TiO_2/p-Si junction (negative on Al/TiO_2 and positive on Si), and W is the thickness of the substrate. The wafer thickness for these diodes was 1000 μm.

We neglect recombination in the substrate bulk because of the high lifetime. With 4 nm 250°C N_2-annealed TiO_2 deposited on both sides, an effective lifetime of 740 μs was measured using the quasi-steady-state photoconductance decay method. Independent experiments show that our lowest interface recombination at the p-Si/TiO_2 interface is ~50 cm/s, implying a lower bound for the bulk lifetime in the substrate of 2.8 ms. The transit time for an electron to cross the 1-mm base, $W^2/2D$, is ~0.15 ms. Thus a "short base model" for electron current is appropriate. The modeled injected electron current, which depends on the substrate doping level, is similar to the measured total current. Thus, the hole current, which is the difference between these two, is small. The goal of this paper is to directly measure this hole current.

III. TiO_2/p-Si/n-Si Heterojunction Bipolar Transistor

Consider an HBT where the n^+ emitter of a conventional n^+/p/n device [see Fig. 3(a)] is replaced with an Al/TiO_2 selective contact [see Fig. 3(b)]. As in the conventional bipolar junction transistor (BJT) device, under forward bias on the emitter–base and reverse or zero bias on the base–collector, electrons are injected into the p-type base, diffuse across the base, and are collected to become collector current (I_C). Hole current from base to emitter (I_B) originates from the base contact. The total current across the emitter–base junction, the emitter current (I_E), is the same as the total current across an Al/TiO_2/Si heterojunction device.

Thus, the hole current, representing processes 2 and 3 in Fig. 1, can be measured as base current I_B, independent of the electron current across the selective contact, assuming negligible leakage at the base–collector junction. I_B can also include base region recombination, an issue that will be addressed later in the paper. This independent measurement of electron and hole currents was not possible with the diode device of Fig. 2.

The HBT device was fabricated by starting with an epitaxial p-type base (doping of 5×10^{14} cm^{-3}, width of 6 μm) on an n-type substrate (doping of 3×10^{18} cm^{-3}) (see Fig. 4). The area of the base–collector junction was isolated by mesa etching. Shadow masks were used to define the areas of the silver base contact, the TiO_2 deposition, and the Al emitter contact. The TiO_2 was deposited as with the diode using a low-temperature chemical vapor deposition utilizing titanium tert-butoxide as the precursor. TiO_2 thickness was measured by a J.A. Woollam spectroscopic ellipsometer and the data were fitted to a vendor-supplied Tauc–Lorentz oscillator model. The emitter area was 0.1 cm $\times$ 0.1 cm, and the base area was 0.35 cm $\times$ 0.35 cm.

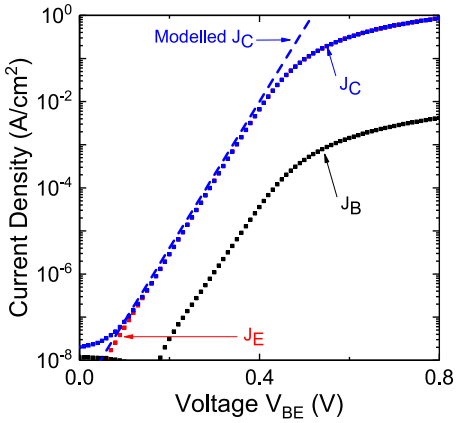

Fig. 5. Gummel plot of J_C and J_B versus base–emitter bias for the HBT of Fig. 4, for $V_{\rm BC} = 0$. J_E is shown in red, J_C in blue, and J_B in black.

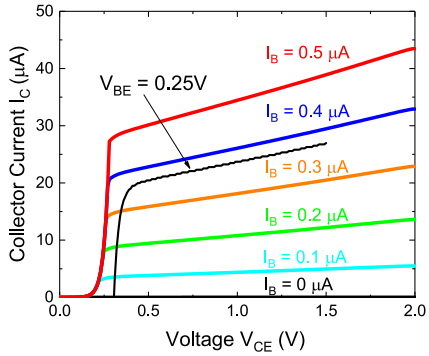

Fig. 6. Common-emitter curve of TiO_2 HBT.

HBT Gummel plots of J_C and J_B versus $V_{\rm BE}$ in forward-active mode ($V_{\rm BC} = 0$ V) for TiO_2 thickness equal to 4.1 nm are shown in Fig. 5. Before the effects of series resistance, the collector current has an ideal slope of ideality factor $n = 1.0$, while the slope of the base current reflects $n = 1.12$. The current gain (collector current /base current ratio) is as large as ∼220. As the base current is so small in comparison to the collector current, the emitter current matches the collector current for almost the entirety of the plot.

However, our focus here is not to make a practical transistor, but rather to isolate different current mechanisms. The large collector current density in Fig. 5 represents electrons injected from emitter to base and diffusing across the base. A dotted line is shown modeling this current with the classical equation for collector current (J_C), assuming 100% base transport factor

$$J_C = \frac{qn_i^2 D_n}{N_A W_B}\left(e^{\frac{qV_{\rm BE}}{kT}} - 1\right) = J_{0,c} * \left(e^{\frac{qV_{\rm BE}}{kT}} - 1\right) \qquad (2)$$

where N_A is the base doping (5×10^{14} cm^{-3}), and W_B is the neutral base width (6 μm). Note that replacing N_A and W_B with substrate doping and substrate thickness would give the diode electron current of (1).

The base current density (J_B) of the device is far smaller than J_C, and represents the current of holes from the p-type base to the emitter contact (Si/TiO_2 selective contact mechanisms 2 and 3 in Fig. 1), as well as any possible recombination of electrons in the base. To see if recombination is significant, Fig. 6 shows the classic common-emitter curves for the HBT (I_C versus $V_{\rm CE}$ for base current steps of 0.1 μA). A current gain of ∼50 is seen. The reduction of I_C below $V_{\rm CE} \sim 0.25$ V is expected for a low common-base current gain in the reverse direction α_R, caused by the large base–collector area versus base–emitter area ratio. I_C rises in reverse bias because of modulation of the base width by $V_{\rm CE}$ (the Early effect). This rise can have two origins: as the base narrows (for a fixed $V_{\rm BE}$), the collector current rises because of a higher electron concentration gradient in the base; and if the base current is dominated by recombination in the neutral base, reducing the base width will reduce the base current for fixed $V_{\rm BE}$. In Fig. 6, in addition to the usual curves of I_C for fixed I_B, we add one curve of I_C for fixed $V_{\rm BE}$ (0.25 V). As $V_{\rm CE}$ increases, the neutral base width narrows because of an increase in the base–collector depletion region, and the resulting steeper electron gradient causes an increase in I_C [13]. In the case of a curve for fixed $V_{\rm BE}$, as the fractional base width decreases, I_C increases by the same fraction. However, what one usually portrays are curves for fixed I_B. In this case, Early pointed out that there is a second effect if the base current is dominated by recombination in the base. The fractional decrease in the base width would cause the base current to decrease. $V_{\rm BE}$ must then increase to raise the electron concentration on the emitter side of the base by the same base width reduction fraction, to keep the base current fixed. This further increases I_C compared with the fixed $V_{\rm BE}$ effect.

It follows (See Appendix) that the ratio of the slopes of I_C versus $V_{\rm CE}$ for fixed I_B versus fixed $V_{\rm BE}$ conditions for a given I_C is

$$\left\{\frac{\frac{dI_C}{dV_{\rm CE}}\big|_{\text{fixed } I_B}}{\frac{dI_C}{dV_{\rm CE}}\big|_{\text{fixed } V_{\rm BE}}}\right\} = 1 + \frac{I_{B,\,\text{recomb}}}{I_B}. \qquad (3)$$

From the data of Fig. 6, this ratio of the slopes is determined to be at most 1.05. From (3), implying at most only 5% of the base current is because of recombination of electrons in the neutral base. Thus, we reach the important conclusion that the base current I_B represents hole current at the selective contact—mechanism 2 and 3.

IV. Relevance for Photovoltaic Devices

The diode in Fig. 2 and the HBT in Fig. 5 were fabricated simultaneously. The total diode current density is given by

$$J_{\rm total\_diode} = (J_{p0} + J_{n0,\rm diode}) * \left(e^{\frac{qV}{kT}} - 1\right) \qquad (4)$$

where $J_{n0,diode}$ is $J_{0,e}$ in (1). The total HBT emitter current density is given by

$$J_E = (J_{p0} + J_{n0,\rm HBT}) * \left(e^{\frac{qV_{\rm BE}}{kT}} - 1\right) \qquad (5)$$

where $J_{n0,HBT}$ is the collector current saturation density $J_{0,c}$ in (2). The base current density J_B is given by

$$J_B = J_{p0} * \left(e^{\frac{qV_{\rm BE}}{kT}} - 1\right). \qquad (6)$$

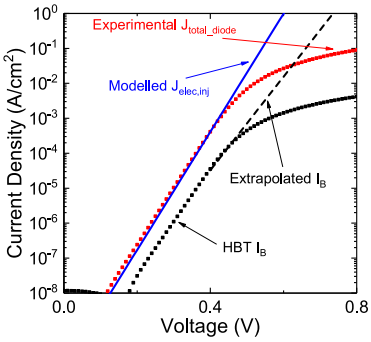

Fig. 7. *J–V* of rectifying selective contact and modeled electron current of Fig. 2, along with base current of HBT representing hole current at the p-Si/TiO_2/Al selective contact.

Thus, from (4) to (6), we see that the base current of the HBT represents the hole current from substrate to the cathode of the diode device of Fig. 2, specifically recombination at the p-Si/TiO_2 interface and/or tunneling either into or through the TiO_2 layer (processes 2 and 3 of Fig. 1). To show the utility of this approach for photovoltaic (PV), in Fig. 7 the HBT J_B is overlaid on the rectifying selective contact diode current of Fig. 2. (The roll-off of the HBT J_B above $V_{\rm BE} = 0.5$ V is because of excessive lateral base resistance). One can extrapolate the exponential region of J_B to relevant voltages for PV (≥ 0.6 V). Near $V = 0.4$ V, the HBT base current (hole current in the selective contact) is $\sim 12\times$ smaller than the electron current. Or, in other words, the hole current is 8% of the total current, thus proving TiO_2/Si is an electron-selective contact and quantifying what the hole current component is. At higher voltages, utilizing the extrapolated HBT base current (assuming the ideality factor < 0.4 V continues up to 0.6 V) and the modeled electron injection current, we obtain even better ratios. For example, at the PV-relevant voltage of 0.6 V, the electron current component is 70 times larger than the hole current component. Thus, considering the structure of Fig. 1 as a PV device, to reduce dark current to raise $V_{\rm OC}$, one either needs to introduce an electron blocking selective contact (or p/p^+ junction) at the substrate Ohmic contact, or use higher substrate doping. If the device of Fig. 2 was therefore improved to reduce the electron dark current by $\sim 11\times$, the hole current and electron dark currents would be comparable. This implies an improved selective contact to reduce hole current would then be necessary for substantial further dark current reduction.

To further show the utility of the HBT approach for independently measuring hole current in an electron-selective contact, both HBTs and diodes, as in Fig. 2, were made with different TiO_2 thicknesses (2.8–8.6 nm). Fig. 8(a) shows a HBT J_B current versus $V_{\rm BE}$ for the different thicknesses. Initially, as the TiO_2 thickness increases, the hole current drops. This is to be expected as tunneling current is reduced (mechanism (3) in Fig. 1) and/or as surface passivation is improved [7], [14]. For the diode with TiO_2 thickness of 3.8 nm, space-charge region recombination dominates at low current levels (the second diode in a typical two-diode model). The comparison of HBT J_B to the diode devices (with diode current at $V = 0.3$ V) is shown in Fig. 8(b).

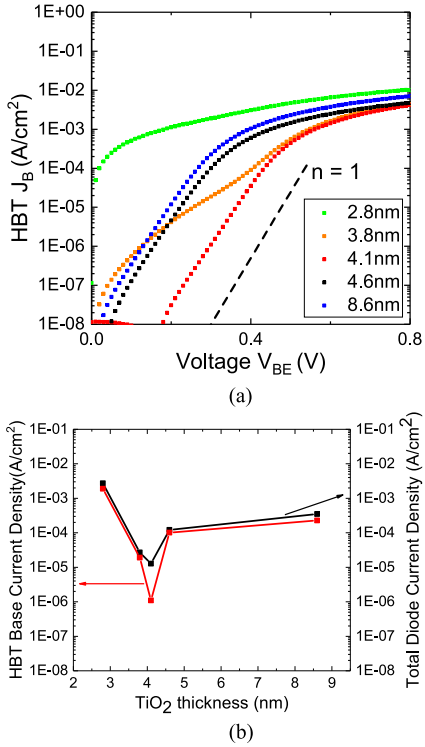

Fig. 8. (a) HBT base current J_B in forward-active mode, representing hole current at the p-Si/TiO_2/Al selective contact for different TiO_2 thicknesses (from 2.8 to 8.6 nm). The dotted line denotes a slope with an ideality factor of 1. (b) Comparison of hole current from p-Si to Al/TiO_2 emitter contact (HBT J_B from Fig. 7) at $V_{\rm BE} = 0.3$ V, and diode current in rectifying selective contacts (p-Si/TiO_2/Al) as in Fig. 2 for forward bias = 0.3 V) for TiO_2 thicknesses from 2.8 to 8.6 nm.

For TiO_2 thickness below 4.1 nm, the diode current matches the HBT base current, showing that the diode is dominated by the hole current. At 4.1 nm, note the hole current is at its minimum, and the PV devices are dominated by electron current. For TiO_2 thicknesses above 4.1 nm, the base current (hole current) and the diode current rise quickly again, and again the diode device is dominated by hole current. This shows there is a narrow TiO_2 thickness window for the performance of a p-Si/TiO_2/Al selective contact from a PV point of view.

The perhaps counter-intuitive increase of hole current at high TiO_2 thickness will be explored in detail elsewhere. In brief however, although not the focus of this paper, one possible explanation for the rise of the hole current is the presence of negative charge in the TiO_2 layer, which has been observed in the literature [15]. Negative charge would push the silicon bands up at the TiO_2/Si interface, thereby reducing the barrier holes see and thus increasing the hole current component caused by mechanism (2) in Fig. 2 (a lower barrier would enable more holes to get to the interface where they could recombine at interface states). To test this hypothesis, current–voltage–temperature (*I–V–T*) measurements were done on the HBTs with TiO_2 thickness 4.1, 4.6, and 8.6 nm. From *I–V–T* measurements (not shown) of the HBT I_B current, we were able to extract a Schottky barrier height of 1.01, 0.83 and 0.78 eV, respectively; this validates the hypothesis that with thicker TiO_2, the silicon bands are being pushed up.

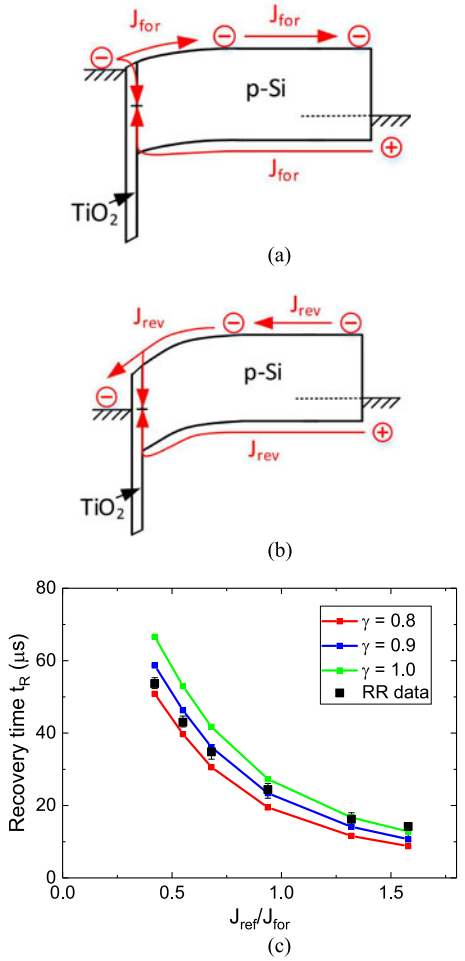

Fig. 9. Reverse recovery experiment. (a) Device under forward bias. (b) Device under initial phase of reverse recovery. (c) Recovery time versus the ratio between forward and reverse current with modeled fitting lines with γ equal to 0.8, 0.9, and 1.0.

To provide independent confirmation that the current of the diode of Fig. 2 (4.1-nm TiO_2) is dominated by electron current, we conducted "reverse recovery" experiments. In a reverse recovery experiment, after steady state in forward bias, the voltage of a diode in series with a resistor is switched from positive to negative. In forward bias, electrons accumulate [see Fig. 9(a)], leading to a particular excess electron profile, which in turn determines the electron current. When the applied voltage is rapidly switched to reverse bias, the excess electron profile initially supports a reverse current many orders of magnitude higher than the device reverse-saturation current as the excess carriers are recovered [see Fig. 9(b)], with the current level set by the applied bias and the resistor [16], [17]. However, in time, the stored electrons are depleted and the current decreases. From these measurements and modeling, one can infer the total number of electrons in the substrate in forward bias [18]. A characteristic parameter for reverse recovery experiments is the recovery time (t_r), which is the time at which the reverse current begins to decrease from its initial value.

The minority carrier injection ratio (commonly known as γ) is the ratio between minority carrier (electron) current and total current. In forward bias, recombination of electrons in defects at the Si/TiO_2 interface would cause γ to be reduced—the current of electrons injected into the substrate would be less than that of the total current, and the recovery time would be reduced for a fixed initial forward current. During the recovery phase, interface recombination would further reduce the recovery time [see Fig 9(b)].

Fig. 9(c) shows our recovery time data for different ratios of forward to reverse bias current. Using numerical models [16], one can fit the data to a minority carrier injection ratio γ. Modeled recovery times for three values of γ: 0.8, 0.9, and 1 are shown in Fig. 9(c). Given the quality of the fitting, γ probably lies between 0.85 and 0.95, implying the ratio of hole current [processes (2 and 3 in Fig. 1(b)] is 5%–15% of the total current. This is in excellent agreement with the HBT-extracted result of the hole component being 8% of the total current as inferred from the data of Fig. 7.

V. Conclusion

In this paper, we have introduced an HBT method to distinguish the hole and electron current across carrier selective contacts, thereby demonstrating an avenue to elucidate current mechanisms for further PV silicon engineering. Using this method on a p-Si/TiO_2/Al electron-selective contact, we have shown that for 4.1-nm TiO_2, the electron current in a typical PV device is more than an order of magnitude larger than the hole currents. Reverse recovery experiments confirm the ratio between hole and electron currents. It is also shown that 4.1 nm is the optimal thickness for CVD-deposited TiO_2.

Appendix

We examine the effect of base recombination, which is typically ignored, on the dependence of I_C in bipolar transistors on $V_{\rm CE}$ because of base width modulation in the common-emitter configuration (the Early effect). Beginning with the classical equations, where W_B is the neutral base width

$$I_C = \frac{qn_i^2 D_n}{W_B N_A} e^{\frac{qV_{\rm BE}}{kT}} \tag{A1}$$

and

$$I_B = I_{B2,3} + I_{B,\rm recomb} = \left[I_{B2,3,o} + \frac{qn_i^2 W_B}{2N_A \tau} \right] e^{\frac{qV_{\rm BE}}{kT}} \tag{A2}$$

where $I_{B2,3}$ represents holes injected from base to emitter [processes 2 and 3 in Fig. 1(b)], with its pre-exponential constant $I_{B2,3,o}$. $I_{B,\rm recomb}$ represents holes recombining with injected electrons in the base, τ is the electron lifetime in the base, and the other terms have their usual meanings.

The dependence of I_C on $V_{\rm CE}$ thus comes from possible changes in W_B and in $V_{\rm BE}$

$$\frac{dI_C}{dV_{\rm CE}} = I_C \left[\frac{-1}{W_B} \frac{dW_B}{dV_{\rm CE}} + \frac{q}{kT} \frac{dV_{\rm BE}}{dV_{\rm CE}} \right]. \tag{A3}$$

If $V_{\rm BE}$ is held constant, then the Early effect is described by

$$\frac{dI_C}{dV_{\rm CE}}\Big|_{\text{fixed } V_{\rm BE}} = -\frac{I_C}{W_B} \cdot \frac{dW_B}{dV_{\rm CE}}. \tag{A4}$$

If I_B is held constant, the Early effect depends on whether the source of the base current depends on W_B and thus $V_{\rm CE}$. Let us differentiate (A2) and set the left side $dI_B = 0$ for a fixed I_B condition

$$dI_B = 0 = \frac{dI_{B2,3}}{dW_B}\left[\frac{dI_{B2,3}}{dW_B} + \frac{dI_{B,\rm recomb}}{dW_B}\right] dW_B + \frac{dI_B}{dV_{\rm BE}} dV_{\rm BE} \tag{A5}$$

leading to

$$0 = \left[\frac{dI_{B2,3}}{dW_B} + \frac{I_{B,\rm recomb}}{W_B}\right] dW_B + \frac{q}{kT} I_B\, dV_{\rm BE}. \tag{A6}$$

Note in (A5), I_B is the total base current. The holes either injected to the emitter or recombining at the base–emitter interface [processes (2) and (3)] have no physical dependence on neutral base width, therefore we can set $dI_{B2,3}/dW_B = 0$. Then

$$\frac{dV_{\rm BE}}{dW_B} = -\frac{I_{B,\ \rm recomb}}{I_B}\frac{kT}{q\ W_B}. \tag{A7}$$

Physically, this means that under a fixed I_B condition, when base recombination dominates the base current, if W_B is decreased, $V_{\rm BE}$ must increase to keep the amount of electron charge in the base constant. Using (A6) to substitute for the dependence of $V_{\rm BE}$ on $V_{\rm CE}$ in (A3) gives for the fixed base current condition

$$\frac{dI_C}{dV_{\rm CE}}|_{\rm fixed\ I_B} = -I_C\left[\frac{1}{W_B}\frac{dW_B}{dV_{\rm CE}} + \frac{q}{kT}\frac{I_{B,\ \rm recomb}}{I_B}\frac{kT}{q\ W_B}\frac{dW_B}{dV_{\rm CE}}\right] \tag{A8}$$

leading to

$$\frac{dI_C}{dV_{\rm CE}}|_{\rm fixed\ I_B} = -\frac{I_C}{W_B}\cdot\left[1 + \frac{I_{B,\rm recomb}}{I_B}\right]\frac{dW_B}{dV_{\rm CE}}. \tag{A9}$$

So we then know the ratio of the slopes of I_C versus $V_{\rm CE}$ for fixed I_B versus fixed $V_{\rm BE}$ conditions. It depends on the fraction of the base current due to recombination in the base, with the ratio of slopes varying between 1 and 2

$$\left\{\frac{\frac{dI_C}{dV_{\rm CE}}|_{\rm fixed\ I_B}}{\frac{dI_C}{dV_{\rm CE}}|_{\rm fixed\ V_{BE}}}\right\} = 1 + \frac{I_{B,\ \rm recomb}}{I_B}\ . \tag{A10}$$

Experimentally, the ratio of base recombination to total base current can be found by

$$\frac{I_{B,\rm recomb}}{I_B} = \left\{\frac{\frac{dI_C}{dV_{\rm CE}}|_{\rm fixed\ I_B}}{\frac{dI_C}{dV_{\rm CE}}|_{\rm fixed\ V_{BE}}}\right\} - 1. \tag{A11}$$

REFERENCES

[1] S. De Wolf, A. Descoeudres, Z. C. Holman, and C. Ballif, "High-efficiency silicon heterojunction solar cells: A review," *Green*, vol. 2, no. 1, pp. 7–24, 2012.

[2] M. Taguchi *et al.*, "HITTM cells—High-efficiency crystalline Si cells with novel structure," *Prog. Photovolt.*, vol. 8, no. 5, pp. 503–514, 2000.

[3] K. Yoshikawa *et al.*, "Silicon heterojunction solar cell with interdigitated back contacts for a photoconversion efficiency over 26%," *Nature Energy*, vol. 2, 2017, Art. no. 17032.

[4] K. A. Nagamatsu, S. Avasthi, J. Jhaveri, and J. C. Sturm, "A 12% efficient silicon/PEDOT:PSS heterojunction solar cell fabricated at $<$ 100C," *IEEE J. Photovolt.*, vol. 4, no. 1, pp. 260–264, Jan. 2014.

[5] S. Avasthi *et al.*, "Hole-blocking titanium-oxide/silicon heterojunction and its application to photovoltaics," *Appl. Phys. Lett.*, vol. 102, 2013, Art. no. 203901.

[6] K. A. Nagamatsu *et al.*, "Titanium dioxide/silicon hole-blocking selective contact to enable double-heterojunction crystalline silicon-based solar cell," *Appl. Phys. Lett.*, vol. 106, no. 12, 2015, Art. no. 123906.

[7] X. Yang *et al.*, "High-performance TiO_2-based electron-selective contacts for crystalline silicon solar cells," *Adv. Mater.*, vol. 28, no. 28, pp. 5891–5897, 2016.

[8] X. Yang, P. Zheng, Q. Bi, and K. Weber, "Silicon heterojunction solar cells with electron selective TiOx contact," *Solar Energy Mater. Solar Cells*, vol. 150, pp. 32–38, 2016.

[9] C. Battaglia *et al.*, "Silicon heterojunction solar cell with passivated hole selective MoOx contact," *Appl. Phys. Lett.*, vol. 104, no. 11, 2014, Art. no. 113902.

[10] R. Islam, G. Shine, and K. C. Saraswat, "Schottky barrier height reduction for holes by Fermi level depinning using metal/nickel oxide/silicon contacts," *Appl. Phys. Lett.*, vol. 105, no. 18, 2014, Art. no. 182103.

[11] J. Jhaveri, A. H. Berg, S. Wagner, and J. C. Sturm, "Measurement of TiO_2/p-Si selective contact performance using a heterojunction bipolar transistor with a selective contact emitter," in *Proc. 44th IEEE Photovolt. Spec. Conf.*, 2017.

[12] J. Jhaveri, A. H. Berg, S. Wagner, and J. C. Sturm, "Al/TiO_2/p-Si heterojunction as an ideal minority carrier electron injector for silicon photovoltaics," in *Proc. 43rd IEEE Photovolt. Spec. Conf.*, 2016, pp. 2444–2447.

[13] J. M. Early, "Effects of space-charge layer widening in junction transistors," *Proc. IRE*, vol. 40, no. 11, pp. 1401–1406, Nov. 1952.

[14] J. Cui *et al.*, "Titanium oxide: A re-emerging optical and passivating material for silicon solar cells," *Solar Energy Mater. Solar Cells*, vol. 158, pp. 115–121, 2016.

[15] A. F. Thomson and K. R. McIntosh, "Light-enhanced surface passivation of TiO_2-coated silicon," *Prog. Photovolt., Res. Appl.*, vol. 20, no. 3, pp. 343–349, 2012.

[16] R. H. Kingston, "Switching time in junction diodes and junction transistors," *Proc. IRE*, vol. 28, no. 5, pp. 829–834, May 1954.

[17] A. S. Grove and C. T. Sah, "Simple analytical approximations to the switching times in narrow base diodes," *Solid State Electron.*, vol. 7, no. 1, pp. 107–110, 1964.

[18] A. H. Berg, K. A. Nagamatsu, and J. C. Sturm, "Extraction of front-and rear-interface recombination in silicon double-heterojunction solar cells by reverse bias transients," *IEEE Trans. Electron Devices*, vol. 64, no. 11, pp. 4518–4525, Nov. 2017.

Janam Jhaveri (S'13) received the B.S. degree in electrical engineering from Purdue University, West Lafayette, IN, USA, in 2011, and the M.A. degree in electrical engineering, in 2013, from Princeton University, Princeton, NJ, USA, where he is currently working toward the Ph.D. degree in electrical engineering.

In 2014, he received the Maeder Graduate Fellowship in Energy and the Environment, and in 2016, he was named a Siebel Scholar in Energy. His research interests include silicon/organic and silicon/metal oxide heterojunctions for photovoltaic applications.

Alexander H. Berg (S'15) was born in New York, NY, USA, in 1991. He received the B.S. degree in engineering physics from Brown University, Providence, RI, USA, in 2013, and the M.A. degree in electrical engineering, in 2015, from Princeton University, Princeton, NJ, USA, where he is currently working toward the Ph.D. degree in electrical engineering.

His research interests include the modeling and material science of hybrid silicon heterojunctions for photovoltaic applications.

James C. Sturm (S'81–M'85–SM'95–F'01) was born in Berkeley Heights, NJ, USA, in 1957. He received the B.S.E. degree in electrical engineering and engineering physics from Princeton University, Princeton, NJ, USA, in 1979, and the M.S. and Ph.D. degrees in electrical engineering from Stanford University, Stanford, CA, USA, in 1981 and 1985, respectively.

In 1979, he joined the Intel Corporation, Santa Clara, CA, USA, as a Microprocessor Design Engineer, and in 1981, he was a Visiting Engineer with Siemens, Munich, Germany. In 1986, he joined the faculty of Princeton University, where he is currently the Stephen R. Forrest Professor in Electrical Engineering. From 2003 to 2015, he was the founding director of the Princeton Institute for the Science and Technology of Materials, and from 1994 to 1995, he was a von Humboldt Fellow with the Institut fuer Halbleitertechnik, University of Stuttgart, Stuttgart, Germany. He has worked in the fields of silicon-based heterojunctions, thin-film and flexible electronics, photovoltaics, the nano-bio interface, three-dimensional integration, and silicon-on-insulator.

Dr. Sturm is a member of the American Physical Society and the Materials Research Society, and was a National Science Foundation Presidential Young Investigator. He is the recipient of more than ten awards for teaching excellence. In 1996 and 1997, he was the Technical Program Chair and General Chair, respectively, of the IEEE Device Research Conference. He was on the organizing committee of IEDM (1988–1992 and 1998–1999), having chaired both the solid-state device and detectors/sensors/displays committees. He was on the Boards of Directors of the Materials Research Society and the Device Research Conference, and was a cofounder of Aegis Lightwave.